International Journal of Automotive Technology, Vol. 24, No. 1, pp. 115–127 (2023)
DOI 10.1007/s12239–023–0011–z

pISSN 1229–9138/ eISSN 1976–3832

OPTIMUM DESIGN CONSIDERING MAIN OPERATING POINTS OF EV TRACTION MOTOR FOR TORQUE RIPPLE REDUCTION AND FUEL ECONOMY IMPROVEMENT

Seok-Won Woo[1,2)], Jin-Cheol Park[3)], Moo-Hyun Sung[2)], Ye-Na Bae[2)], Jongsun Yoon[2)], Kyoung-Soo Cha[3)] and Myung-Seop Lim[3)*]

[1)]Motor Development Department, LG Magna e-Powertrain Co., Ltd., 322 Gyeongmyeong-daero, Seo-gu, Incheon 22744, Korea
[2)]Department of Automotive Engineering (Automotive-Computer Convergence), Hanyang University, Seoul 04763, Korea
[3)]Department of Automotive Engineering, Hanyang University, Seoul 04763, Korea

(Received 3 March 2022; Revised 13 May 2022; Accepted 6 July 2022)

ABSTRACT–In this paper, the optimum design considering main operating points (MOPs) of the electric vehicle (EV) traction motor is conducted to reduce the torque ripple and improve the fuel economy. MOPs of the traction motor can be determined by considering ratios of number of operating points or considering energy consumption ratios based on the EV simulation. Specifically, the optimum design is conducted with the aim of minimizing the torque ripples at MOPs determined by considering ratios of number of operating points (RNOMOPs) and maximizing the inverter-motor system efficiencies at MOPs determined by considering energy consumption ratios (ECRMOPs) to simultaneously reduce the torque ripple and improve the fuel economy. To verify the effectiveness of the optimum design considering MOPs proposed in this paper, torque ripples at RNOMOPs and the fuel economies according to the initial model and the optimum model are compared. As a result, torque ripples of the optimum model at RNOMOPs are remarkably decreased by 58.84 %p and 57.77 %p, respectively, and the fuel economy according to the optimum model is improved by 1.72 %. Conclusively, the effectiveness of the optimum design considering MOPs of the EV traction motor for the torque ripple reduction and the fuel economy improvement is verified.

KEY WORDS : Electric vehicle, Fuel economy, Main operating point, Optimum design, System efficiency, Torque ripple, Traction motor

1. INTRODUCTION

In recent years, regulations on internal combustion engine vehicles (ICEVs) have become stricter due to the global environmental pollution (Tu *et al*., 2019; Taljegard *et al*., 2019). To comply with this phenomenon, demands for an eco-friendly vehicle such as electric vehicles (EVs) are increased (De Santiago *et al.*, 2012; Sarlioglu *et al.*, 2017). Generally, in EVs, batteries, inverters, and traction motors replace fuel tanks and engines used in ICEVs.

Among various types of the EV traction motors, the interior permanent magnet synchronous motors (IPMSMs) where permanent magnets (PMs) are inserted in the rotor are widely used owing to advantages of high efficiency, high power density, and high speed driving. This is because the IPMSM can use not only magnetic torque but also reluctance torque due to the difference in inductance magnitude between *d*-axis and *q*-axis. However, the reluctance torque leads to an inevitable torque ripple which affects the noise and vibration (Gieras *et al.*, 2006; Jung *et al.*, 2018). Thus, because of the existence of the reluctance torque, the IPMSM have relatively many issues related to the noise and vibration. Therefore, since the noise and vibration of the EV can cause the insecurity of the vehicle and the discomfort of passengers, etc., it is necessary to reduce the torque ripple of the IPMSM for EV traction (Ge *et al*., 2017; Gieras *et al.*, 2006).

Furthermore, batteries take a long time to be fully charged and have a low energy density (Wen *et al*., 2020). Accordingly, various studies about improving the fuel economy of the EV have been actively performed to increase the mileage, reducing the energy consumption. (Cha *et al.*, 2020; Cha *et al.*, 2021; Chin *et al.*, 2021; Hwang *et al.*, 2021). To improve the fuel economy of the EV, it is necessary to increase the efficiency of the actuating system such as the inverter and traction motor.

In this paper, the optimum design considering main operating points (MOPs) of the IPMSM for EV traction is conducted to reduce the torque ripple of the traction motor and improve the fuel economy of the EV. The operating

**Corresponding author*. e-mail: myungseop@hanyang.ac.kr

points of the traction motor and the fuel economy of the EV can be easily predicted by using the EV simulation according to certain driving cycle. Based on the EV simulation, MOPs of the traction motor can be determined by considering the ratios of number of operating points or considering the energy consumption ratios of the inverter-motor system (Woo *et al.*, 2021).

If the torque ripples of the traction motor at operating points with high number of operations are increased, the noise and vibration characteristics of the EV are deteriorated while certain driving cycle is completed. Thus, it is necessary to reduce the torque ripples at MOPs determined by considering the ratios of number of operating points (RNOMOPs). Additionally, the inverter-motor system efficiencies (Hereinafter, 'system efficiencies') at operating points with high energy consumption are closely related to the fuel economy of the EV. Thus, it is necessary to increase the system efficiencies at MOPs determined by considering the energy consumption ratios (ECRMOPs) for the fuel economy improvement of the EV. Specifically, in this paper, the optimum design is conducted with the aim of minimizing the torque ripples at RNOMOPs and the maximizing the system efficiencies at ECRMOPs to simultaneously reduce the torque ripple and improve the fuel economy of the EV. Finally, in order to verify the effectiveness of the optimum design considering MOPs of the traction motor proposed in this paper, the torque ripples at RNOMOPs, system efficiencies at ECRMOPs, and the fuel economies of the EV according to the initial model and the optimum model are compared.

2. INVERTER-MOTOR SYSTEM EFFICIENCY

To precisely predict the fuel economy of the EV, it is necessary to consider the system efficiency reflecting the inverter losses as well as the motor losses.

In this chapter, first, the method of calculating the motor losses is explained. Next, the method of mathematically calculating the inverter losses is explained. Finally, the calculation method of the system efficiency considering losses of the inverter and losses of the traction motor is explained.

2.1. Motor Losses

The losses of PM motors are mainly composed of the copper loss, core loss, PM eddy current loss, and mechanical loss. In this paper, only copper loss and core loss which account for most of the losses of the PM motors are considered. Besides, in the case of the copper loss, the effects of AC resistance generated by the skin effect and proximity effect are neglected in this paper.

2.1.1. Armature copper loss

The armature phase resistance can be calculated as follows:

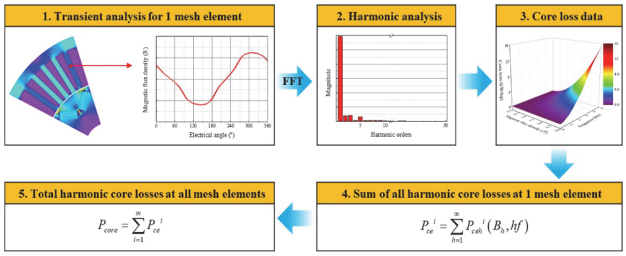

Figure 1. Calculation process of core loss.

$$R_a = \rho_0 \{1 + \alpha (T - T_0)\} \frac{N_{ph} l_{winding}}{A_{coil} n_{parallel}} \quad (1)$$

where R_a is the armature phase resistance; ρ_0 is the resistivity of a conductor when the temperature is T_0; α is the temperature coefficient of the resistivity; N_{ph} is the series turns per phase; $l_{winding}$ is the length of 1-turn winding; A_{coil} is the cross-sectional area of a conductor; and $n_{parallel}$ is the number of parallel circuits.

The armature copper loss can be calculated as follows:

$$P_{copper} = m \cdot I_a^2 \cdot R_a \quad (2)$$

where P_{copper} is the armature copper loss; m is the number of phases; and I_a is the armature phase current.

2.1.2. Core loss

Figure 1 shows the calculation process of the core losses by using 2-dimensional (2D) electromagnetic finite element analysis (FEA). The calculation process of the core losses is as follows (Park and Lim, 2019):

a) The magnetic flux density is calculated by each mesh element for electrical one period by using the transient analysis.
b) Harmonic analysis by using fast Fourier transform (FFT) is performed to obtain the harmonic components of the previously calculated magnetic flux density.
c) The experimental data of the core loss according to frequency and magnetic flux density of the core material is used.
d) The sum of all harmonic core losses at each mesh element for electrical one period is calculated based on the experimental data of the core loss.
e) The total harmonic core losses of the traction motor are obtained by adding all harmonic core losses calculated at each mesh element.

2.2. Inverter Losses

The inverter is a power conversion device which generates alternative current (AC) power from direct current (DC) power by using semiconductor switching devices. Figure 2 shows the structure of the conventional 3-phase 2-level Wye-connection

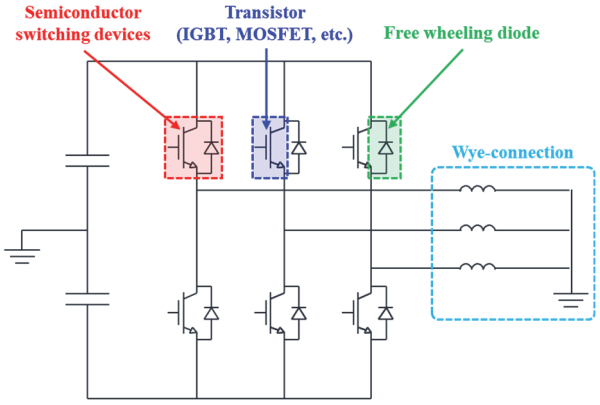

Figure 2. Structure of conventional 3-phase 2-level Wye-connection inverter.

inverter. As shown in Figure 2, the insulated gate bipolar transistor (IGBT) or the metal oxide semiconductor field effect transistor (MOSFET) are mainly used as transistors. Also, the free-wheeling diodes are used to protect transistors.

A pulse width modulation (PWM) technique is used to create the gating pulses for turning semiconductor switching devices on or off so that the inverter can generate a fundamental wave voltage which has the equivalent magnitude and frequency of the voltage command (Kim, 2017). When semiconductor switching devices are turned on or off by the PWM technique, the conduction loss and the switching loss are generated. In this paper, the conduction loss and the switching loss of semiconductor switching devices are mathematically calculated by considering the characteristics of the semiconductor switching devices.

2.2.1. Armature copper loss

Since semiconductor switching devices are not ideal, the internal resistance exists. Also, semiconductor switching devices should exceed specific threshold voltage to be conducted. Because of these characteristics, the conduction loss of the inverter occurs. Assuming that the current flowing through the semiconductor switching device is fairly constant over one PWM cycle, the waveform of the armature phase current is sinusoidal, and the motor is operated within the linear modulation range, the conduction losses of the transistor and the free-wheeling diode can be calculated as follows (Berringer *et al.*, 1995; Llorente, 2020):

$$P_{cond(T)} = \left(\frac{1}{2\pi} + \frac{\mathrm{MI}\cdot\cos\phi}{8}\right)V_{CE0}I_a + \left(\frac{1}{8} + \frac{\mathrm{MI}\cdot\cos\phi}{3\pi}\right)r_{CE}I_a^2 \tag{3}$$

$$P_{cond(D)} = \left(\frac{1}{2\pi} - \frac{\mathrm{MI}\cdot\cos\phi}{8}\right)V_{F0}I_a + \left(\frac{1}{8} - \frac{\mathrm{MI}\cdot\cos\phi}{3\pi}\right)r_F I_a^2 \tag{4}$$

where $P_{cond(T)}$ and $P_{cond(D)}$ are the conduction losses of transistor and the free-wheeling diode, respectively; MI is the modulation index; ϕ is the power factor angle; V_{CE0} is the collector-emitter threshold voltage of the transistor; V_{F0} is the forward voltage drop of the diode; r_{CE} is the internal resistance of the transistor; r_F is the internal resistance of the free-wheeling diode; and I_a is the armature phase current.

V_{CE0}, r_{CE}, V_{F0}, r_F can be obtained by referring to the characteristic information in the data sheet of the semiconductor switching device to be used.

2.2.2. Switching loss

Generally, semiconductor switching devices need the energy required to be switched, and a high switching frequency increases the number of switches. Therefore, the switching loss of the semiconductor switching device is proportional to the switching frequency and the switching energy. The average switching losses of the transistor and the free-wheeling diode can be calculated as follows (Berringer *et al.*, 1995; Llorente, 2020):

$$P_{sw(T)} = f_{SW}\frac{E_{on}(I_a) + E_{off}(I_a)}{\pi}\left(\frac{V_d}{V_{d,ref}}\right) \tag{5}$$

$$P_{sw(D)} = f_{SW}\frac{E_{rr}(I_a)}{\pi}\left(\frac{V_d}{V_{d,ref}}\right) \tag{6}$$

where $P_{sw(T)}$ and $P_{sw(D)}$ are the switching losses of the transistor and the free-wheeling diode, respectively; f_{sw} is the switching frequency; E_{on} and E_{off} are the energy for turning the transistor on and off; E_{rr} is the reverse recovery energy of the free-wheeling diode; V_d is the dc link voltage; and $V_{d,ref}$ is the test voltage for calculating the switching loss.

$E_{on}(I_a)$, $E_{off}(I_a)$, $E_{rr}(I_a)$ can be obtained by referring to the characteristic information in the data sheet of the semiconductor switching device to be used.

2.3. Inverter-Motor System Efficiency

The efficiencies of the motor, inverter, and inverter-motor system can be expressed as follows:

$$\eta_{motor} = \frac{P_{motor\_out}}{P_{motor\_in}} \tag{7}$$

$$\eta_{inverter} = \frac{P_{inverter\_out}}{P_{inverter\_in}} = \frac{P_{motor\_in}}{P_{inverter\_in}} \tag{8}$$

$$\eta_{system} = \frac{P_{motor\_out}}{P_{inverter\_in}} = \eta_{motor}\cdot\eta_{inverter} \tag{9}$$

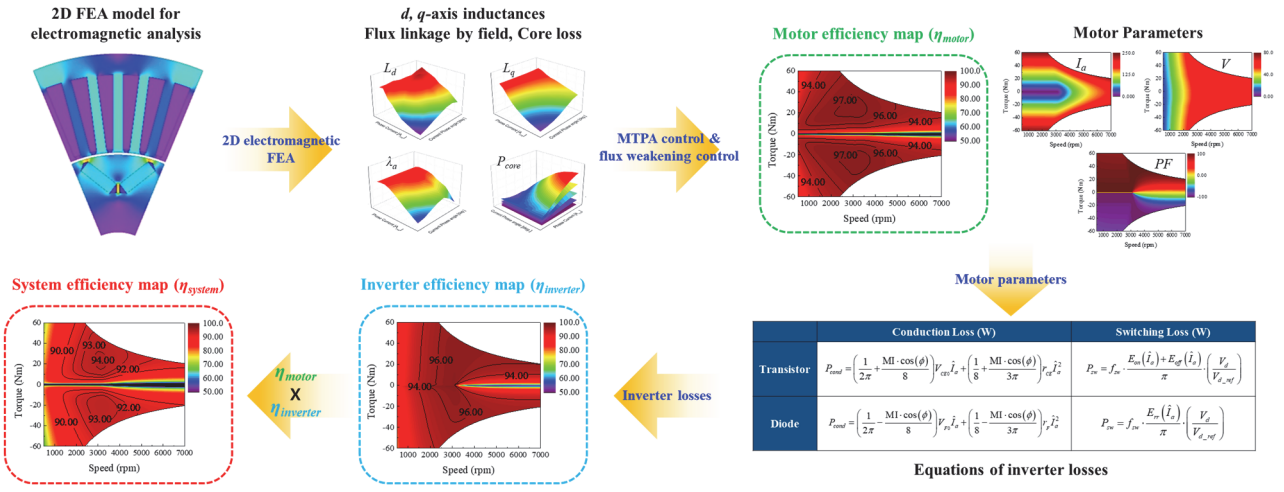

Figure 3. Calculation process of inverter-motor system efficiency.

where η_{motor} is the efficiency of the traction motor; P_{motor_in} and P_{motor_out} are the input power and the output power of the traction motor, respectively; $\eta_{inverter}$ is the efficiency of the inverter; $P_{inverter\_in}$ and $P_{inverter\_out}$ are the input power and the output power of the inverter, respectively; and η_{system} is the system efficiency.

Based on the calculation methods of the motor losses and the inverter losses explained in chapter 2, the overall calculation process of the system efficiency conducted in this paper is shown in Figure 3 (Cha, 2022).

A) By using the 2D electromagnetic FEA, *d*-, *q*-axis inductances, flux linkage by the field, and core loss of the target motor model are analyzed.
B) Based on the analyzed data, the motor efficiency and motor parameters such as the armature current, line to line voltage, power factor are determined by applying the maximum torque per ampere (MTPA) control and flux weakening control.
C) Determined motor parameters are considered in the inverter loss equations explained in section 2.2 to calculate the total losses of the inverter.
D) The system efficiency is calculated by considering both the motor efficiency and the inverter efficiency.

3. MAIN OPERATING POINTS OF TRACTION MOTOR

To perform the optimum design considering MOPs of the traction motor, MOPs should be previously determined. Based on the EV simulation, MOPs can be determined by using two methods (Hereinafter, 'method 1 and method 2'). From the method 1, RNOMOPs related to the torque ripple can be determined by considering the ratios of number of operating points. From the method 2, ECRMOPs related to the fuel economy can be determined by considering the energy consumption ratios.

Table 1. Specifications of target vehicle.

Items		Value	Unit
Curb weight		474	kg
Length		2,338	mm
Width		1,237	mm
Height		1,454	mm
Wheelbase		1,686	mm
Wheel radius		330	mm
Air drag coefficient		0.64	-
Battery capacity		6.1	kWh
Gear	Ratio	9.23	-
	Efficiency	95	%

The EV modeling for the EV simulation is developed by using the Powertrain Blockset library provided in MATALB/Simulink. Since this paper focuses on obtaining the energy consumption of the inverter-motor system and fuel economy of the EV, only the longitudinal dynamic characteristics of the vehicle are considered (Kim, 2021). The target vehicle used for the EV simulation is Renault Twizy, and the specifications are listed in Table 1. Also, the gear efficiency is assumed as 95 %. Additionally, since Twizy is suitable for urban driving rather than highway driving owing to the low maximum torque and power of the traction motor, New York city cycle (NYCC) driving cycle is used to perform the EV simulation assuming the urban driving situations of light-duty vehicles.

In this chapter, first, the longitudinal dynamic characteristics of the vehicle is explained. Next, based on the EV modeling developed by using the Powertrain Blockset library, the overall process of the EV simulation is explained. Finally,

the method 1 and method 2 for determining MOPs of the traction motor are explained in detail.

3.1. Longitudinal Dynamic Characteristics of Vehicle

In this paper, the EV simulation is performed based on the longitudinal dynamic characteristics of the vehicle (Cha *et al*., 2020; Cha *et al*., 2021; Eshani *et al.*, 2005; Woo *et al*., 2021). The motion of the vehicle is affected by the resistive force and the tractive force. The longitudinal dynamic forces acting on the vehicle climbing the slope are shown in Figure 4. The resistive force acting on the vehicle consists of the rolling resistive force, the grade resistive force, and the aerodynamic drag force. Thus, the total resistive force can be expressed as follows:

$$\begin{aligned} F_{res} &= F_R + F_G + F_A \\ &= f_R M_v \cos\theta + M_v g \sin\theta + \frac{1}{2}\rho A_F C_D \left(V_v - V_w\right)^2 \end{aligned} \tag{10}$$

where F_{res} is the total resistive force; F_R is the rolling resistive force; F_G is the grade resistive force; F_A is the aerodynamic drag force; f_R is the rolling resistance coefficient; M_v is the vehicle mass; θ is the longitudinal slope angle; g is the gravitational acceleration; ρ is the air density; A_f is the frontal area; C_D is the aerodynamic drag coefficient; V_v is the vehicle speed; and V_w is the wind speed.

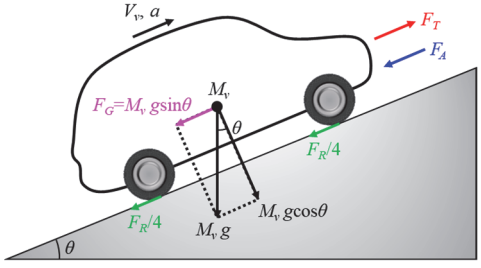

Figure 4. Longitudinal dynamic force diagram of vehicle.

Both the tractive force and the resistive force determine the dynamic behavior of the vehicle. The motion equation of the vehicle is expressed as follows:

$$M_v a = F_T - F_{res} \tag{11}$$

where F_T is the tractive force; and a is the acceleration of the vehicle.

The required torque for the EV traction is expressed as follows:

$$T_M = \frac{r_w F_T}{n_G \eta_G} \tag{12}$$

where T_M is the motor torque; r_w is the wheel radius; n_G is the gear ratio; and η_G is the gear efficiency.

The rotational speed of the traction motor is expressed as follows:

$$\omega_M = \frac{n_G V_v}{r_w} \tag{13}$$

where ω_M is the rotational speed of the traction motor.

3.2. Process of EV Simulation

In this section, the overall process of the EV simulation is explained based on the EV modeling shown in Figure 5.

A) The longitudinal Driver Model block is used to reflect the driver's intention according to given driving cycle. The longitudinal Driver Model block receives the target speed from the driving cycle. Based on a proportional integral (PI) control, the longitudinal Driver Model block estimates the acceleration and deceleration commands to eliminate speed error between the target speed and the current speed of the vehicle. The longitudinal Driver Model block generates acceleration command if the current speed of the vehicle is less than the target speed, and generates deceleration command if

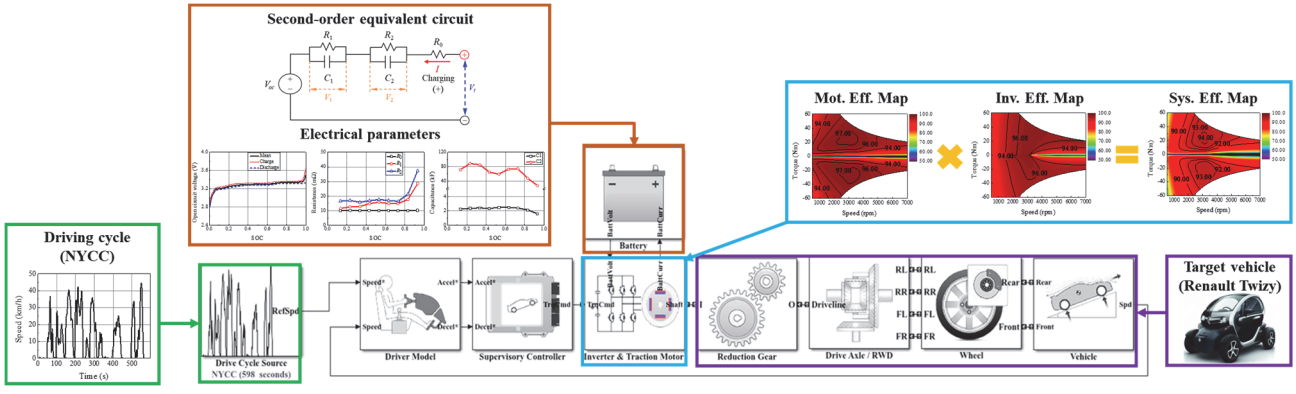

Figure 5. Schematic of EV modeling developed by using Powertrain Blockset library in MATLAB/Simulink.

the current speed of the vehicle is greater than the target speed. Then, the acceleration and deceleration commands are transmitted to the Supervisory Controller block.

B) The Supervisory Controller block generates the required torque command according to the acceleration and deceleration commands based on the generating and motoring speed-torque curve of the traction motor. Then, the torque command is transmitted to the Inverter & Traction Motor block.

C) The Inverter & Traction Motor block needs the system efficiency map to calculate the battery input power required for generating the torque command. Based on the system efficiency map, the input power of the battery is calculated by considering the mechanical output power of the traction motor. Then, the battery current to generate the input power of the battery is transmitted to the Battery block.

D) To calculate the battery voltage according to the battery current, the second-order equivalent circuit model shown in Figure 6 is used (Cha *et al.*, 2020; Hu *et al.*, 2011; Klein and Park, 2017; Perez *et al.*, 2016). This equivalent circuit model is suitable for the EV applications where both charging and discharging occur. It consists of open-circuit voltage (V_{oc}), two resistance-capacitor (RC) pairs (R_1, C_1, R_2, C_2), and ohmic resistance (R_0). The state-space model of the battery equivalent circuit model is as follows (Cha *et al.*, 2020; Hu *et al.*, 2011; Perez *et al.*, 2016):

$$\frac{d\mathrm{SOC}}{dt}(t) = \frac{I(t)}{C_{bat}} \tag{14}$$

$$\frac{dV_1}{dt}(t) = -\frac{V_1(t)}{R_1C_1} + \frac{I(t)}{C_1} \tag{15}$$

$$\frac{dV_2}{dt}(t) = -\frac{V_2(t)}{R_2C_2} + \frac{I(t)}{C_2} \tag{16}$$

$$V_t(t) = V_{oc}(\mathrm{SOC}) + V_1(t) + V_2(t) + R_0I(t) \tag{17}$$

where SOC means the state of charge of the battery; I is the batter current (positive for charging, negative for discharging); V_1 and V_2 are the voltages across the two RC pairs; C_{bat} is the nominal capacity; and V_t is the terminal voltage.

Figure 7 shows the electrical parameters of the battery equivalent circuit model which are experimentally obtained (Cha *et al.*, 2020; Perez *et al.*, 2016). Based on the Equations (14) ~ (17) and the electrical parameters shown in Figure 7, the battery voltage according to the battery current is calculated, and then fed back to the Inverter & Traction Motor block.

E) The motor torque generated through this process is transmitted to each wheel via the reduction gear and the drive axle for operating the vehicle. Finally, the current speed of the vehicle is again fed back to the longitudinal Driver Model block.

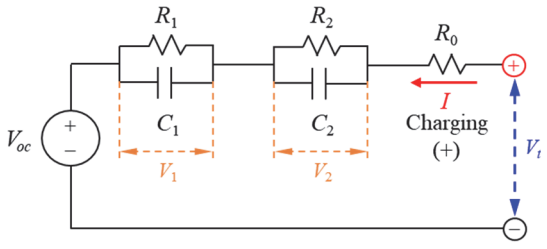

Figure 6. Second-order equivalent circuit of battery.

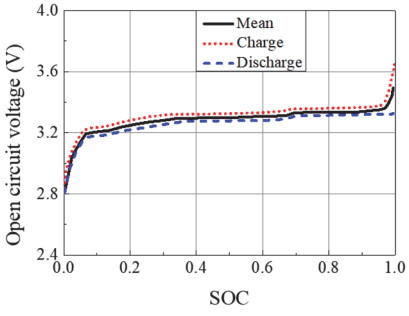

(a)

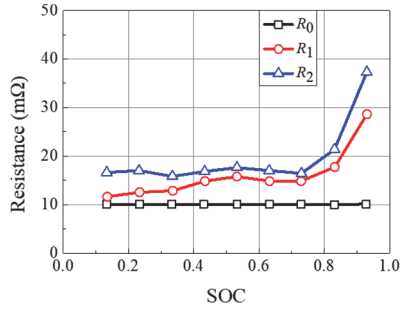

(b)

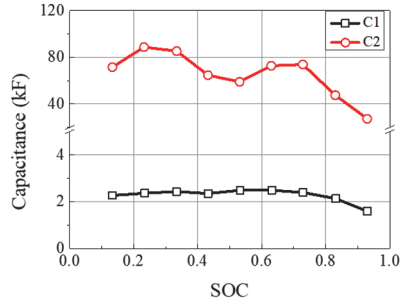

(c)

Figure 7. Electrical parameters of second-order battery equivalent circuit: (a) Open circuit voltage; (b) Resistance; (c) Capacitance.

As a result of performing the EV simulation according to NYCC driving cycle based on the EV modeling developed in this paper, it is confirmed that the vehicle speed follows the target speed from NYCC driving cycle well as shown in Figure 8.

3.3. Two Methods for Determining Main Operating Points of Traction Motor

All operating points of the traction motor are distributed as shown in Figure 9 by performing the EV simulation in consideration of the specifications of the target vehicle and the driving cycle. Based on all operating points of the traction motor, the method 1 and the method 2 for determining MOPs of the traction motor will be explained in detail.

From the method 1, RNOMOPs related to the torque ripple are determined by considering the ratios of the number of operating points at operating regions. The ratios of the number of operating points at generating and motoring regions are calculated as follows (Woo *et al*., 2021):

$$RNO_{Gen,i} = \frac{n_{Gen,i}}{\sum_{i=1}^{k_{Gen}} n_{Gen,i}} \tag{18}$$

$$RNO_{Mot,j} = \frac{n_{Mot,j}}{\sum_{j=1}^{k_{Mot}} n_{Mot,j}} \tag{19}$$

where $RNO_{Gen,i}$ and $RNO_{Mot,j}$ are the ratios of the number of operating points at the i-th generating region and the j-th motoring region, respectively; k_{Gen} and k_{Mot} are the number of all generating regions and all motoring regions, respectively; and $n_{Gen,i}$ and $n_{Mot,j}$ are the number of operating points at the i-th generating region and the j-th motoring region, respectively.

Figure 10 shows the ratios of the number of operating points at generating and motoring regions calculated by using Equations (18) and (19). Among them, as shown in Figure 10, the operating regions where the ratio of the number of operating points is greater than 8 % are determined as main operating regions (green).

From the method 2, ECRMOPs related to the fuel economy are determined by considering the energy consumption ratios of the inverter-motor system at operating regions. The energy consumption ratios at generating and motoring regions are calculated as follows (Woo *et al*., 2021):

$$ECR_{Gen,i} = \frac{\left(T_{Gen,i}\omega_{Gen,i}\right)t_{Gen,i}}{\sum_{i=1}^{k_{Gen}}\left(T_{Gen,i}\omega_{Gen,i}\right)t_{Gen,i}} \tag{20}$$

$$ECR_{Mot,j} = \frac{\left(T_{Mot,j}\omega_{Mot,j}\right)t_{Mot,j}}{\sum_{j=1}^{k_{Mot}}\left(T_{Mot,j}\omega_{Mot,j}\right)t_{Mot,j}} \tag{21}$$

where $ECR_{Gen,i}$ and $ECR_{Mot,j}$ are the energy consumption ratios at the i-th generating region and the j-th motoring region, respectively; k_{Gen} and k_{Mot} are the number of all generating regions and all motoring regions, respectively; $T_{Gen,i}$ and $T_{Mot,j}$ are the torques at the i-th generating region and the j-th motoring region, respectively; $\omega_{Gen,i}$ and $\omega_{Mot,j}$ are the rotational speeds at the i-th generating region and the j-th motoring region, respectively; and $t_{Gen,i}$ and $t_{Mot,j}$ are the operating times for the period of 598s which is the duration time of NYCC driving cycle at the i-th generating region and the j-th motoring region, respectively.

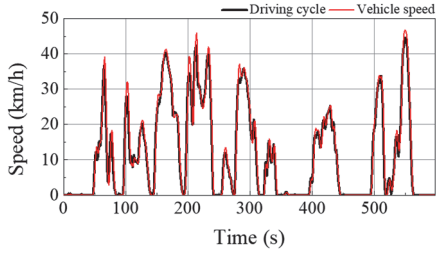

Figure 8. Driving cycle (NYCC) and vehicle speed.

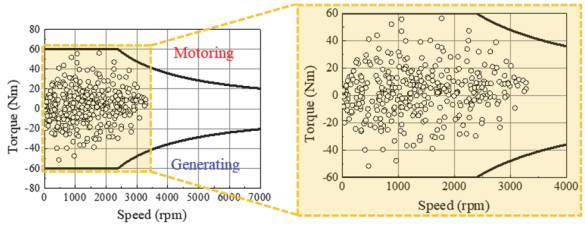

Figure 9. All operating points of traction motor.

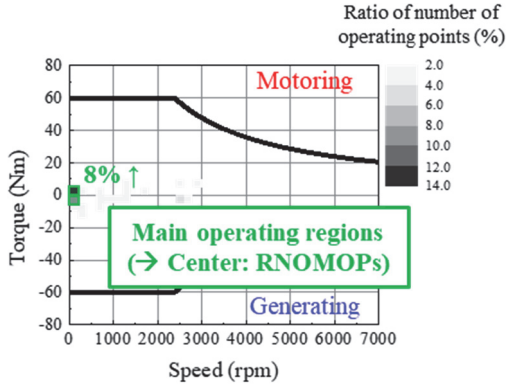

Figure 10. Ratio of number of operating points.

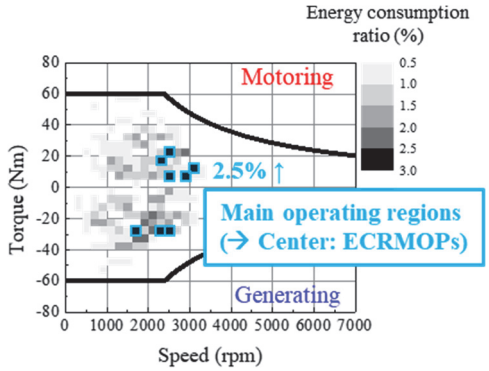

Figure 11. Energy consumption ratio.

Table 2. Main operating points of traction motor determined by using method 1 and method 2.

Method	Main operating points (MOPs)	Speed (rpm)	Torque (Nm)
Method 1	RNOMOP 1	100	-2.5
	RNOMOP 2	100	2.5
Method 2	ECRMOP 1	1700	-27.5
	ECRMOP 2	2300	-27.5
	ECRMOP 3	2500	-27.5
	ECRMOP 4	2300	17.5
	ECRMOP 5	2500	7.5
	ECRMOP 6	2500	22.5
	ECRMOP 7	2900	7.5
	ECRMOP 8	3100	12.5

Figure 11 shows the energy consumption ratios at generating and motoring regions calculated by using Equations (20) and (21). Among them, as shown in Figure 11, the operating regions where the energy consumption ratio is greater than 2.5 % are determined as main operating regions (sky-blue).

We regard MOPs of the traction motor as the centers of main operating regions. Accordingly, MOPs of the traction motor are determined by using the method 1 and the method 2 as shown in Table 2. As shown in Table 2, two RNOMOPs are determined by using the method 1, and eight ECRMOPs are determined by using the method 2.

4. OPTIMUM DESIGN OF TRACTION MOTOR

In this paper, the optimum design considering MOPs of the IPMSM for EV traction is conducted to reduce the torque ripple of the traction motor and improve the fuel economy of the EV. Specifically, based on the multi-objective function, the optimum design is conducted with the aim of minimizing the torque ripples at RNOMOPs and maximizing the system efficiencies at ECRMOPs to simultaneously reduce the torque ripple and improve the fuel economy of the EV.

In this chapter, first, the initial model to perform the optimum design and the design variables are explained. Then, the process of the optimum design considering MOPs of the traction motor proposed in this paper is explained. Next, the optimum design is performed to create the optimum model. Finally, by comparing the torque ripples at RNOMOPs, system efficiencies at ECRMOPs, and the fuel economies of the EV according to the initial model and the optimum model, the effectiveness of the optimum design considering MOPs of the traction motor proposed in this paper is verified.

4.1. Initial Model

The configuration and the speed-torque curve of the initial model to perform the optimum design are shown in Figures 12 and 13, respectively. Also, the specifications of the initial model are listed in Table 3. The motor type of the initial model is double-layer v-type IPMSM with 8 poles and 48 slots. The maximum torque and maximum power are 60 Nm and 15 kW, respectively. The series turns per phase and the stack length are 12 turns and 130 mm, respectively. Additionally, the type of the semiconductor switching device used in this paper is FS660R08A6P2FLB (IGBT).

4.2. Process of Optimum Design

Figure 14 shows the design variables to be optimized. We select design variables related to the system efficiency and the torque ripple as follows: PM thickness (X_1), PM width (X_2), PM pole angle (X_3), Rib thickness (X_4), Rib angle (X_5), Bridge thickness (X_6), Tooth tip thickness (X_7), Shoe height (X_8), Slot opening width (X_9), Series turns per phase (X_{10}), Stack length (X_{11}). The process of the optimum design considering MOPs of the traction motor conducted in this paper is shown in Figure 15.

A) As the design of experiments (DOE), Latin hypercube sampling technique which is a statistical method used to uniformly place the experimental points in multi-dimensional experimental regions without repetition is used (Viana *et al.*, 2010; Kim *et al.*, 2018). Specifically, the optimal Latin hypercube design (OLHD) and the sequential maximin distance design (SMDD) are used. For the OLHD and the SMDD, the maximin distance criterion is applied. By the OLHD, 180 experimental points which have space-filling and non-collapsing properties in experimental regions are determined. Next, the SMDD is applied by considering experimental points which were pre-determined by the OLHD, and 120 experimental points are determined. Thus, by the OLHD and the SMDD, 300 experimental points are determined.

B) The torque ripples at RNOMOPs, and the system efficiencies at ECRMOPs are analyzed for each experimental point based on the 2D electromagnetic FEA and the calculation process of the system efficiency.

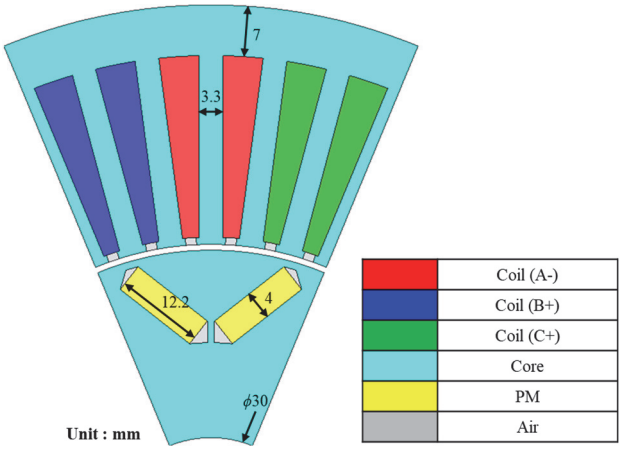

Figure 12. Configuration of initial model.

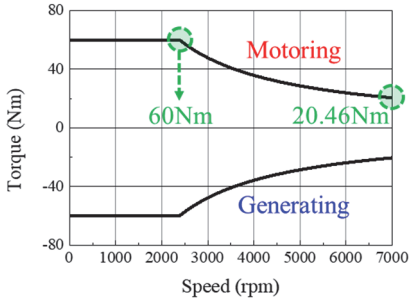

Figure 13. Speed-torque curve of initial model.

Table 3. Specifications of initial model.

Items		Value	Unit
Pole / slot		8 / 48	-
Shape	PM pole angle	29.25	°
	Rib thickness	1	mm
	Rib angle	2.5	°
	Bridge thickness	1	mm
	Tooth tip thickness	1	mm
	Slot opening width	1.5	mm
	Stack length	130	mm
Power specification	DC link voltage	66	V_{dc}
	Current limit	300 ↓	A_{rms}
Motor performance	Maximum torque	60	Nm
	Maximum power	15	kW
	Maximum speed	7000	rpm
Core	Material	35PN230	-
PM	Material	N42H	-
Coil	Series turns per phase	12	-
	Parallel circuits	4	-
	Fill factor	37	%
	Current density	12 ↓	A_{rms}/mm^2

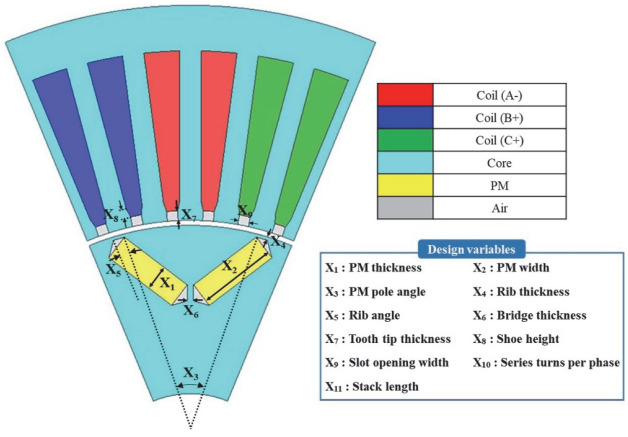

Figure 14. Design variables to be optimized.

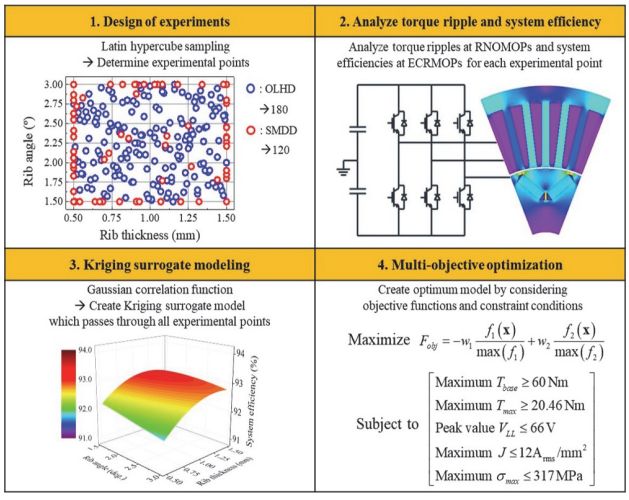

Figure 15. Process of optimum design.

C) By using Gaussian correlation function, the correlations between the responses for each experimental point are obtained. Based on the correlations, the Kriging surrogate models passing through all experimental points are created (Kim *et al.*, 2020).

D) Based on the created Kriging surrogate models, the multi-objective optimization is conducted by considering the objective functions. In this paper, the objective functions are the minimization of the torque ripples at RNOMOPs (Hereinafter, 'objective function 1') and the maximization of the system efficiencies at ECRMOPs (Hereinafter, 'objective function 2'). In consideration of these two objective functions, the multi-objective optimization is conducted by using the multi-objective function expressed as follows:

$$\text{Maximize } F_{obj} = -w_1 \frac{f_1(\mathbf{x})}{\max(f_1)} + w_2 \frac{f_2(\mathbf{x})}{\max(f_2)} \quad (22)$$

where F_{obj} is the multi-objective function; **x** is the matrix of design variables; f_1 and f_2 are the response of Kriging surrogate models of torque ripples at RNOMOPs and the response of Kriging surrogate models of system efficiencies at ECRMOPs, respectively; and w_1 and w_2 are the weighting factors of the objective function 1 and the objective function 2, respectively.

As expressed in Equation (22), the multi-objective function is maximized as the torque ripples at RNOMOPs are minimized or the system efficiencies at ECRMOPs are maximized. Therefore, in this paper, the multi-objective optimization is conducted with the aim of maximizing the multi-objective function by using in-house codes. Additionally, since both the objective function 1 and the objective function 2 are important, the ratio of w_1 to w_2 are determined as 1:1.

In addition to the objective functions, the constraint conditions should be considered. First, the optimum model should satisfy the maximum torque and maximum power specifications of the traction motor required to operate the EV. Thus, we consider the maximum torques at the base speed and the maximum speed as constraint conditions. Also, the peak value of the line to line voltage is considered in this paper due to the voltage limitation caused by the battery usage in the EV. Specifically, if the peak value of the line to line voltage under load conditions is higher than the DC link voltage of the inverter, the inverter cannot apply the required magnitude or waveform of the current. Additionally, we consider the maximum current density for preventing damage to the armature coil caused by the heat generation. Also, we consider the maximum stress of the rotor at the maximum speed to prevent the rotor from scattering. Specifically, both the yield strength of the core material and safety factor of 1.2 are considered. As a result, constraint conditions considered in this paper can be expressed as follows:

$$\text{subject to} \begin{bmatrix} \text{Maximum } T_{base} \geq 60\,\text{Nm} \\ \text{Maximum } T_{max} \geq 20.46\,\text{Nm} \\ \text{Peak value } V_{LL} \leq 66\,\text{V} \\ \text{Maximum } J \leq 12\,\text{A}_{\text{rms}}/\text{mm}^2 \\ \text{Maximum } \sigma_{max} \leq 317\,\text{MPa} \end{bmatrix} \tag{23}$$

where T_{base} and T_{max} are the torques at the base speed and the maximum speed, respectively; V_{LL} is the line to line voltage; J is the current density; and σ_{max} is the stress of the rotor at maximum speed.

Finally, in consideration of objective functions and constraint conditions, the multi-objective optimization is conducted with the aim of maximizing the multi-objective function to create the optimum model by using in-house codes.

4.3. Result of Optimum Design

The configurations of the initial model and the optimum model are shown in Figure 16. The specifications of the optimum model are listed in Table 4. To verify the effectiveness of the optimum design considering MOPs of the traction motor proposed in this paper, torque ripples at RNOMOPs, system efficiencies at ECRMOPs, and the fuel economies of the EV according to the initial model and the optimum model are compared.

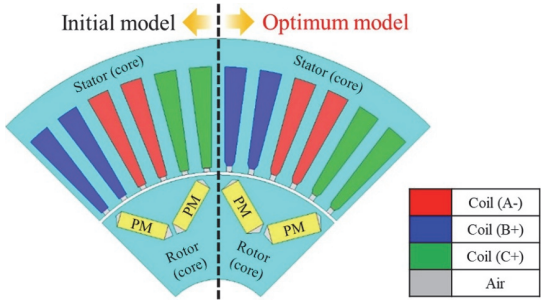

Figure 16. Configurations of initial model and optimum model.

Table 4. Specifications of optimum model.

Items		Value	Unit
Pole / slot		8 / 48	-
Shape	PM thickness	12.5	mm
	PM width	5	mm
	PM pole angle	30.26	°
	Rib thickness	1	mm
	Rib angle	2.27	°
	Bridge thickness	1	mm
	Tooth tip thickness	1.5	mm
	Shoe height	1.1	mm
	Slot opening width	1.41	mm
	Stack length	110	mm
Power specification	DC link voltage	66	V_{dc}
	Current limit	225 ↓	A_{rms}
Motor performance	Maximum torque	60	Nm
	Maximum power	15	kW
	Maximum speed	7000	rpm
Core	Material	35PN230	-
PM	Material	N42H	-
Coil	Series turns per phase	16	-
	Parallel circuits	4	-
	Fill factor	37	%
	Current density	12 ↓	A_{rms}/mm^2

The torque waveforms with the torque ripple values of the initial model and the optimum model at RNOMOPs are shown in Figure 17. As shown in Figure 17, the torque ripple of the optimum model at (100 rpm, -2.5 Nm) is remarkably decreased by 58.84 %p from 88.28 to 29.44 %. Also, the torque ripple of the optimum model at (100 rpm, 2.5 Nm) is remarkably decreased by 58.77 %p from 87.54 to 28.77 %.

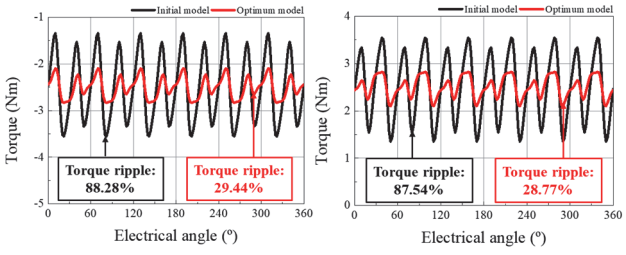

(a) (b)

Figure 17. Torque waveform and torque ripple of initial model and optimum model at RNOMOPs: (a) 100 rpm, -2.5 Nm; (b) 100 rpm, 2.5 Nm.

The efficiency maps of the motor, inverter, and inverter-motor system of the initial model and the optimum model are shown in Figures 18 and 19, respectively. Also, the maps of the difference between the initial model and the optimum model in the efficiency of the motor, inverter, and inverter-motor system are shown in Figure 20 with ECRMOPs. As shown in Figure 20 (a), it is confirmed that the motor efficiencies of the optimum model are higher than those of the initial model at only three ECRMOPs. However, as shown in Figure 20 (b), the inverter efficiencies of the optimum model are higher than those of the initial model at six ECRMOPs. This is because the current required to

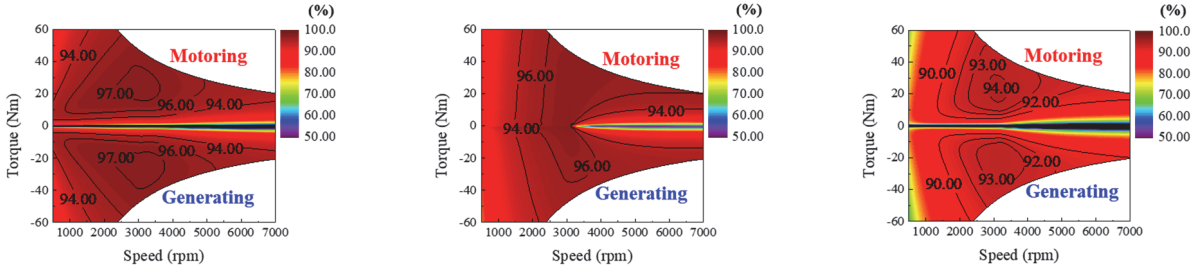

(a) (b) (c)

Figure 18. Efficiency map of initial model: (a) Motor; (b) Inverter; (c) Inverter-motor system.

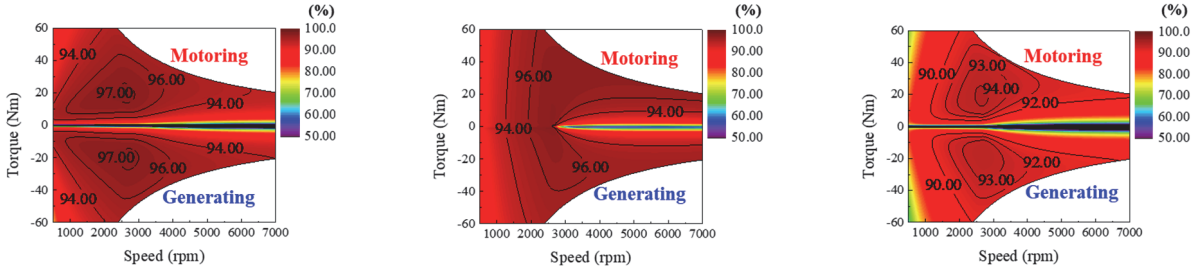

(a) (b) (c)

Figure 19. Efficiency map of optimum model: (a) Motor; (b) Inverter; (c) Inverter-motor system.

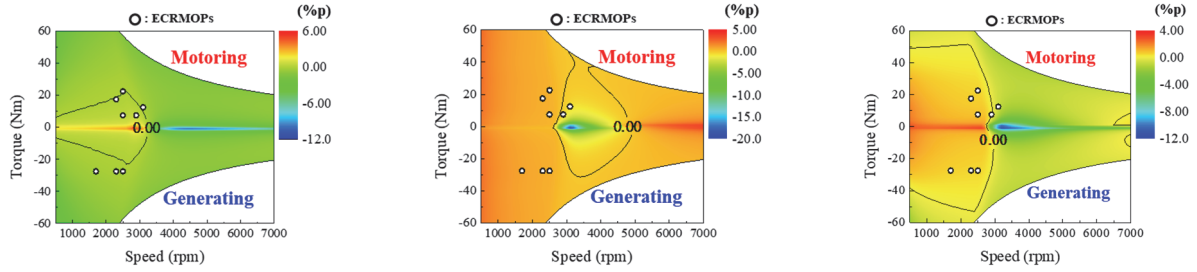

(a) (b) (c)

Figure 20. Efficiency difference map (Optimum model - Initial model): (a) Motor; (b) Inverter; (c) Inverter-motor system.

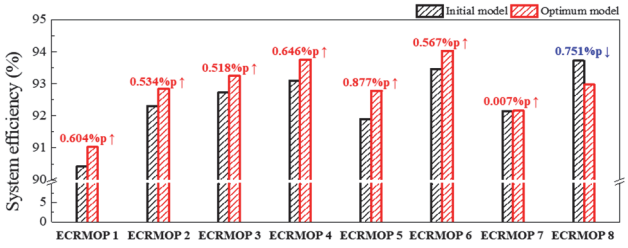

Figure 21. System efficiencies of initial model and optimum model at ECRMOPs.

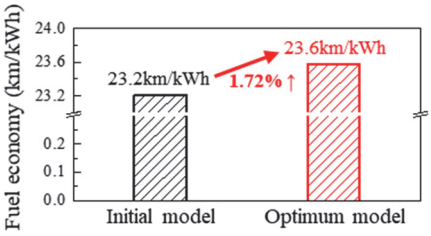

Figure 22. Fuel economies of EV according to initial model and optimum model.

generate the specific torque is decreased due to the increase of the series turns per phase. According to this tendency, as shown in Figure 20 (c), the system efficiencies of the optimum model are higher than those of the initial model at most ECRMOPs. Specifically, the system efficiencies at eight ECRMOPs of the initial model and the optimum model are shown in Figure 21. As shown in Figure 21, except for the system efficiency at only one ECRMOP, the system efficiencies of the optimum model are higher than those of the initial model. Since the system efficiencies of the optimum model are increased at most ECRMOPs, it is expected that the fuel economy of the EV according to the optimum model is also improved.

The fuel economy of the EV represents the battery power consumed for the mileages until the EV completes the driving cycle. Thus, the fuel economy of the EV can be calculated as follows:

$$\text{Fuel economy} = \frac{\int_0^{t_f} v_{veh}\, dt}{\int_0^{t_f} V_{bat} I_{bat}\, dt} \tag{24}$$

where t_f is the taken time to complete the driving cycle; v_{veh} is the velocity of the vehicle; and V_{bat} and I_{bat} are the voltage and the current consumed in the battery, respectively.

The fuel economies of the EV according to the initial model and the optimum model are shown in Figure 22. As shown in Figure 22, the fuel economy of the EV according to the optimum model is improved by 1.72 % from 23.2 to 23.6 km/kWh. This is because the system efficiencies of the optimum model are increased at most ECRMOPs.

Therefore, it is confirmed that the torque ripples of the optimum model at RNOMOPs are remarkably decreased, and the fuel economy of the EV according to the optimum model is improved, compared with the initial model. Conclusively, the effectiveness of the optimum design considering MOPs of the IPMSM for EV traction to reduce the torque ripple and improve the fuel economy is verified.

5. CONCLUSION

In this paper, the optimum design considering MOPs of the EV traction motor for the torque ripple reduction and the fuel economy improvement is proposed. MOPs of the traction motor are determined by using the method 1 and the method 2 based on the EV simulation. From the method 1, RNOMOPs related to the torque ripple are determined by considering the ratios of number of operating points. From the method 2, ECRMOPs related to the fuel economy are determined by considering the energy consumption ratios.

The optimum model is created by conducting the multi-objective optimization with the aim of minimizing the torque ripples at RNOMOPs and maximizing the system efficiencies at ECRMOPs to simultaneously reduce the torque ripple and improve the fuel economy of the EV. Then, the torque ripples at RNOMOPs, system efficiencies at ECRMOPs, and the fuel economies of the EV according to the initial model and the optimum model are compared. As a result, it is confirmed that the torque ripples of the optimum model at RNOMOPs are remarkably decreased by 58.84 %p and 58.77 %p, respectively, and the fuel economy of the EV according to the optimum model is improved by 1.72 %, compared with the initial model. Conclusively, the effectiveness of the optimum design considering MOPs of the EV traction motor for the torque ripple reduction and the fuel economy improvement is verified.

ACKNOWLEDGEMENT–This work was supported by the National Research Foundation of Korea (NRF) grant funded by the Korea government (MSIT) (No. NRF-2020R1A4A4079701).

REFERENCES

Berringer, K., Marvin, J. and Perruchoud, P. (1995). Semiconductor power losses in AC inverters. *IEEE Industry Applications Conf. Thirtieth IAS Annual Meeting*, Orlando, FL, USA.

Cha, K. S. (2022). Optimization of EV Model with Multi-Mode Powertrain System through Winding Changeover Motor and 2-Speed Transmission. Ph.D. Dissertation. Hanyang University, Seoul, Korea.

Cha, K. S., Chin, J. W., Park, S. H., Jung, Y. H., Lee, E. C. and Lim, M. S. (2021). Design method for reducing AC resistance of traction motor using high fill factor coil to improve the fuel economy of eBus. *IEEE/ASME Trans. Mechatronics* **26**, **3**, 1260–1270.

Cha, K. S., Kim, D. M., Jung, Y. H. and Lim, M. S. (2020).

Wound field synchronous motor with hybrid circuit for neighborhood electric vehicle traction improving fuel economy. *Applied Energy*, **263**, 114618.

Chin, J. W., Cha, K. S., Park, M. R., Park, S. H., Lee, E. C. and Lim, M. S. (2020). High efficiency PMSM with high slot fill factor coil for heavy-duty EV traction considering AC resistance. *IEEE Trans. Energy Conversion* **36**, **2**, 883–894.

De Santiago, J., Bernhoff, H., Ekergård, B., Eriksson, S., Ferhatovic, S., Waters, R. and Leijon, M. (2011). Electrical motor drivelines in commercial all-electric vehicles: A review. *IEEE Trans. Vehicular Technology* **61**, **2**, 475–484.

Eshani, M., Gao, Y., Gay, S. E. and Emadi, A. (2005). *Modern Electric, Hybrid Electric and Fuel Cell Vehicles. Fundamentals, Theory, and Design*. CRC Press. Boca Raton, Florida, USA.

Ge, X., Zhu, Z. Q., Kemp, G., Moule, D. and Williams, C. (2016). Optimal step-skew methods for cogging torque reduction accounting for three-dimensional effect of interior permanent magnet machines. *IEEE Trans. Energy Conversion* **32**, **1**, 222–232.

Gieras, J. F., Wang, C. and Lai, J. C. (2006). *Noise of Polyphase Electric Motors*. CRC Press. Boca Raton, Florida, USA.

Hu, W., Nian, H. and Sun, D. (2019). Zero-sequence current suppression strategy with reduced switching frequency for open-end winding PMSM drives with common DC bus. *IEEE Trans. Industrial Electronics* **66**, **10**, 7613–7623.

Hu, Y., Yurkovich, S., Guezennec, Y. and Yurkovich, B. J. (2011). Electro-thermal battery model identification for automotive applications. *J. Power Sources* **196**, **1**, 449–457.

Hwang, S. W., Ryu, J. Y., Chin, J. W., Park, S. H., Kim, D. K. & Lim, M. S. (2021). Coupled electromagnetic-thermal analysis for predicting traction motor characteristics according to electric vehicle driving cycle. *IEEE Trans. Vehicular Technology* **70**, **5**, 4262–4272.

Jung, Y. H., Lim, M. S., Yoon, M. H., Jeong, J. S. and Hong, J. P. (2017). Torque ripple reduction of IPMSM applying asymmetric rotor shape under certain load condition. *IEEE Trans. Energy Conversion* **33**, **1**, 333–340.

Kim, D. M. (2021). Modeling and Optimization of Fuel Cell Electric Vehicle Considering Wide Variation of DC Link Voltage to Electric Powertrain and Air Supply System. Ph. D. Dissertation. Hanyang University. Seoul, Korea.

Kim, H., Kim, S., Kim, T., Lee, T. H., Ryu, N., Kwon, K. and Min, S. (2018). Efficient design optimization of complex system through an integrated interface using symbolic computation. *Advances in Engineering Software*, **126**, 34–45.

Kim, S., Lee, S. G., Kim, J. M., Lee, T. H. and Lim, M. S. (2020). Robust design optimization of surface-mounted permanent magnet synchronous motor using uncertainty characterization by bootstrap method. *IEEE Trans. Energy Conversion* **35**, **4**, 2056–2065.

Kim, S. H. (2017). *Electric Motor Control: DC, AC, and BLDC Motors*. 1st edn. Elsevier Science. Cambridge, Massachusetts, USA.

Klein, M. P. and Park, J. W. (2017). Current distribution measurements in parallel-connected lithium-ion cylindrical cells under non-uniform temperature conditions. *J. Electrochemical Society* **164**, **9**, A1893.

Lin, X., Huang, W. and Wang, L. (2018). SVPWM strategy based on the hysteresis controller of zero-sequence current for three-phase open-end winding PMSM. *IEEE Trans. Power Electronics* **34**, **4**, 3474–3486.

Llorente, R. M. (2020). Practical Control of Electric Machines: Model-Based Design and Simulation. Springer. Cham, Switaerland.

Park, H. J. and Lim, M. S. (2019). Design of high power density and high efficiency wound-field synchronous motor for electric vehicle traction. *IEEE Access*, **7**, 46677–46685.

Perez, H. E. (2016). *Model Based Optimal Control, Estimation, and Validation of Lithium-Ion Batteries*. Ph. D. Dissertation. University of California, Berkeley. Berkeley, California, USA.

Sarlioglu, B., Morris, C. T., Han, D. and Li, S. (2016). Driving toward accessibility: a review of technological improvements for electric machines, power electronics, and batteries for electric and hybrid vehicles. *IEEE Industry Applications Magazine* **23**, **1**, 14–25.

Tu, W., Santi, P., Zhao, T., He, X., Li, Q., Dong, L., Wallington, T. J. and Ratti, C. (2019). Acceptability, energy consumption, and costs of electric vehicle for ride-hailing drivers in Beijing. *Applied Energy*, **250**, 147–160.

Taljegard, M., Göransson, L., Odenberger, M. and Johnsson, F. (2019). Impacts of electric vehicles on the electricity generation portfolio–A Scandinavian-German case study. *Applied Energy*, **235**, 1637–1650.

Viana, F. A., Venter, G. and Balabanov, V. (2010). An algorithm for fast optimal Latin hypercube design of experiments. *Int. J. Numerical Methods in Engineering* **82**, **2**, 135–156.

Wen, J., Zhao, D. and Zhang, C. (2020). An overview of electricity powered vehicles: Lithium-ion battery energy storage density and energy conversion efficiency. *Renewable Energy*, **162**, 1629–1648.

Woo, S. W., Cha, K. S., Chin, J. W. and Lim, M. S. (2021). Optimization of traction motor according to main operating points determination methods for high fuel economy of electric vehicles. *24th Int. Conf. Electrical Machines and Systems (ICEMS)*, Gyeongju, Korea.